A laser heating study of the CeO_2 solid/liquid transition: challenges related to a refractory compound with a very high oxygen pressure

L. Capriotti[1], A. Quaini[1,3], R. Böhler[1], K. Boboridis[1], L. Luzzi[2] and D. Manara[1,*]

[1]*European Commission, Joint Research Centre, Institute for Transuranium Elements (ITU), P.O. Box 2340, 76125 Karlsruhe, Germany*
[2]*Politecnico di Milano, Department of Energy, Enrico Fermi Center for Nuclear Studies (CeSNEF), via La Masa 34, 20156 Milano, Italy*
[3]*CEA Saclay – DEN/DANS/DPC/SCCME/LM2T – 91191 Gif-sur-Yvette Cedex, France*

Received: September 1, 2014. Accepted: October 15, 2014.

*Corresponding author: dario.manara@ec.europa.eu

1 INTRODUCTION

CeO_2 has a fluorite-like crystalline structure, in which the main defects are oxygen vacancies. These vacancies increase the catalytic activity [1, 2], making ceria one of the most studied compounds for the implementation of solid-oxide fuel cells [3].

Another important application of CeO_2 is as a surrogate for plutonium dioxide in the nuclear research activities [4–6], which permits to estimate the properties of the latter without radioactivity and radiotoxicity issues. In particular, affinities between CeO_2 and PuO_2 have been observed in the metal–oxygen phase diagram in the region of hypostoichiometric-stoichiometric dioxides [7] (fig. 1a and b). In this part of the Ce-O and Pu-O phase diagrams, the types of defect and the related Gibbs free energy for the fluorite phases are similar. These aspects are described in detail elsewhere [7, 8].

The Ce-O phase diagram is still a matter of discussion. The latest revision by Zinkevich et al. [9] highlighted the complexity of the hypostoichiometric CeO_{2-x} region at low temperature where the appearance of defects in the fluorite structure stabilises many superstructures of fluorite-type lattice, Ce_nO_{2n-2m}. Furthermore, at high temperature, close to the melting temperature of CeO_2, the refractory nature of the compound and the tendency to reduce are emphasised. The melting temperature of CeO_2 is still not well established because of these issues, and different values are reported in the literature. Under reducing atmosphere a value of 2670 K [10] was measured. Foex [11] obtained a higher value of 2753 K using a solar furnace in air. Values of 3073 K and (3000 ± 20) K were attained respectively by Tromble [12] and Brewer [13], although no details about their experimental approaches are available. The former performed the experiments under 16 atm of buffer gas whilst the latter used a pure O_2 atmosphere (at an unspecified pressure).

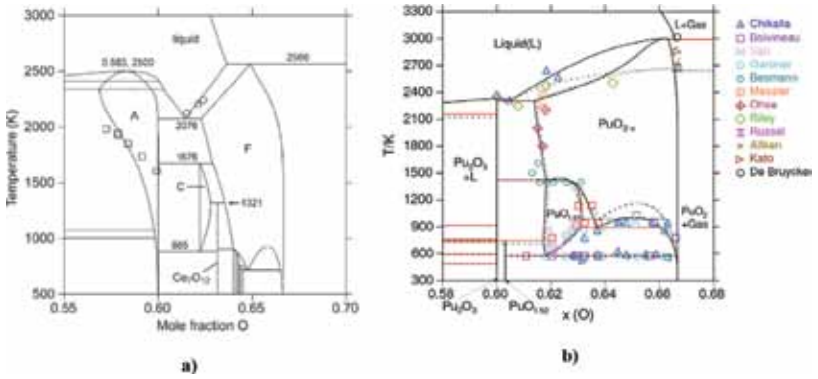

FIGURE 1
a) Phase diagram of the Ce-O system at 0.1 MPa [9]. b) The Pu-O system close to the stoichiometric PuO_2 region [4].

The goal of the present work is to study, by laser heating, the very high temperature behaviour of CeO_2, measuring its melting temperature in different controlled atmospheres (reducing and oxidising). Tests have also been performed with a high overpressure of He (up to 15 MPa), aimed at maintaining CeO_2 as close as possible to stoichiometry upon melting by slowing the vaporisation kinetics. Finally, a general overview of the high-temperature behaviour of ceria under different conditions is given, for the first time, in a single experimental investigation. Interesting analogies between the systems Ce-O and Pu-O are pointed out even in the current high-temperature range.

2 MATERIALS

Commercial Alfa Aesar® 99.998% pure CeO_2 powder was pressed into pellets (8 mm diameter and 2 to 4 mm thick) and sintered under air for 6 h at 1800 K. Samples were then stored under inert atmosphere (dry argon or vacuum) until their melting/freezing point measurements.

Given the low level of impurities in the initial powder, their effect on the melting behaviour, at least within the uncertainty limits of the current approach (see section 3.2), is here considered to be negligible.

X-ray diffraction (XRD) was performed before and after the annealing procedure. The crystalline structure and lattice parameter remained the same in the two cases (5.4080 Å before sintering, 5.4079 Å after sintering) so no changes in the structure or stoichiometry were measurable.

The XRD instrumental details used in this work are reported in section 3.3.

3 EXPERIMENTAL METHODS

3.1 Laser heating technique

The technique employed is laser heating coupled with fast pyrometry [14]. This technique has already been applied to the study of many radioactive and non-radioactive refractory materials [15–17].

An overview of the experimental set-up is shown in fig. 2.

The sample is mounted in a small autoclave closed by a 10 mm-thick gas-proof quartz window and is held in place by three or four graphite screws to obtain quasi-containerless conditions in order to reduce or avoid interaction with the containment. With this facility, during the laser heating experiments samples are held under a slight overpressure (up to 0.3 MPa) of a controlled atmosphere. The chemical environment (reducing, oxidizing) can thus be imposed for each test, while overpressure is needed in order to slow the vaporization kinetics and avoid massive vaporization from the sample surface following the very fast heating process. Oxidizing conditions were produced by filling the autoclave with compressed air. In order to obtain slightly

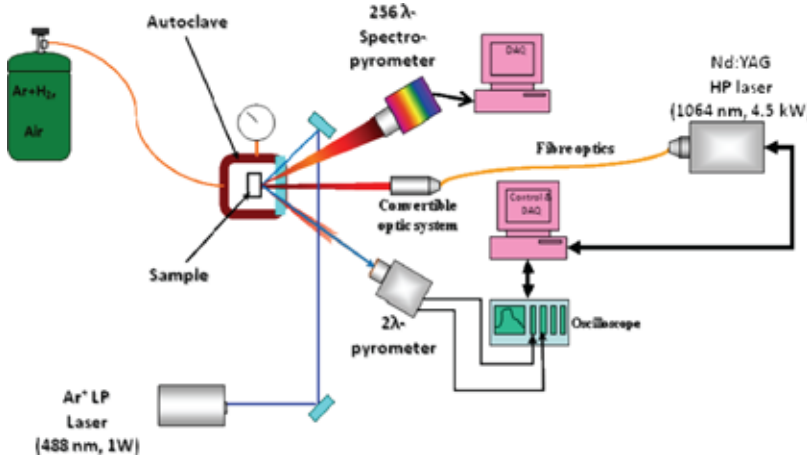

FIGURE 2
Experimental set-up employed in this work.

reducing conditions, instead, compressed argon was mostly used. Such inert gas can be seen as a slightly reducing environment when compared with the high oxygen pressure of ceria.

The heating agent is a Nd: YAG 4.5 KW laser radiating at 1064 nm, coupled to the experimental cell with optical fibers. The laser beam impinged on the sample surface on an approximately circular area of 6 mm in diameter. The thermal analysis was performed on the cooling stage of the cycle after switching off the laser beam.

The sample radiance temperature was measured on a spot of 0.5 mm in diameter at the center of the laser-heated area by means of a fast pyrometer equipped with a logarithmic amplifier (settling time of about 10 μs to 1% of log output) and operating at 650 nm [14]. To obtain the true temperature a spectro-pyrometer is employed to calculate the Normal Spectral Emissivity (NSE). The spectro-pyrometer, based on a linear array of 256 Si photodiodes, was used to record the sample thermal radiance in the range 488 nm – 1011 nm. This instrument allows a more complete spectral analysis, whereby its main disadvantage is in the poorer time resolution (one spectrum per millisecond at best). Due to low signal-to-noise ratio, moreover, only the range of 550 to 920 nm was useful for the current measurements. Radiance spectra recorded on CeO_2 in the vicinity of the melting/solidification point were fitted by least-squares regression to Planck's distribution law for blackbody radiance, modified by a wavelength- and temperature-dependent function assumed to represent the NSE. Although this approach has been proven to be numerically unstable [18], it can be reasonably trusted in electrically insulating materials, like cerium dioxide at high temperature, for which the NSE can

be assumed to be wavelength independent (grey body behaviour). More details about the technique employed are discussed elsewhere [14].

Compared to other techniques, employing a high power laser has the advantage of shortening the time of the experiments and thus reducing vaporization and chemical instability of the compounds.

3.2 High pressure cell

In order to check the highest melting temperature reported in literature for cerium dioxide (around 3000 K under a high, but not specified, pressure of oxygen [12, 13]), a high-pressure facility similar to the one described in [14] was also used. The idea here is to slow as much as possible vaporization kinetics, as described in [14].

The high pressure cell consists of a cylindrical steel container designed to withstand an internal pressure of up to 4000 bar. The vessel contains a pressurised chamber of 1 cm^3, where the specimen is located, connected with the high pressure gas feed system. On top, the chamber is closed by a 1-cm thick sapphire window. The high pressure cell was filled with helium, as it has the best optical characteristics among the inert gases at high pressure [19]. Further details on the high pressure equipment are described elsewhere [20].

3.3 Post-melting sample characterization

Scanning electron microscopy and X-ray diffraction were used to characterise CeO_2 samples after the laser heating/melting/freezing cycles. Melted specimens were recovered for post-melting analysis by SEM (Philips model XL40) and energy-dispersive X-ray spectroscopy (EDX). Cross-sections through melted surfaces were prepared for microstructural analysis and imaged unetched. X-ray diffraction (XRD) was performed in this work using a Bruker® D8 Advance diffractometer (Cu-Ka1 radiation) with a 2θ range of 10°-120° using 0.009° steps with 2 s of count time per step at operating conditions of 40 KV–40 mA. The XRD instrument was equipped with a Lynxeye® 3° linear position sensitive detector.

3.4 Uncertainty analysis

The most significant uncertainty sources have been combined, according to the independent error propagation law [14], and expanded to yield relative temperature uncertainty bands corresponding to 2 standard deviation (k = 2 coverage factor). These uncertainty components stem from our current temperature scale definition δT (i.e. the uncertainty in the pyrometer calibration), the NSE assessment $\delta T_{\varepsilon\lambda}$ and the experimental data scatter on the current phase transition radiance temperature data $\delta T_{\lambda m}$, the latter being the main source of uncertainty:

$$\delta T_m = \sqrt{\delta T^2 + \delta T_{\varepsilon\lambda}^2 + \delta T_{\lambda m}^2} \tag{1}$$

The resulting uncertainty is of the order of 30 K at 3000 K. Exact uncertainty values are reported for each measurement in this work.

4 RESULTS

4.1 Laser melting under 0.3 MPa

The present radiance spectra analysis yielded an average value of 0.90 for the NSE of freezing ceria (figure 3b). This value has then been used to convert the radiance temperatures measured by the pyrometers into real temperatures.

A typical real temperature thermogram measured on CeO_2 is shown in fig. 3a.

During the laser pulse, the temperature rose up to a maximum value of 3200 K. When the laser was switched off, the temperature rapidly decreased producing a clear freezing thermal arrest.

The vessel was filled with argon or air in order to reproduce reducing or oxidising conditions respectively.

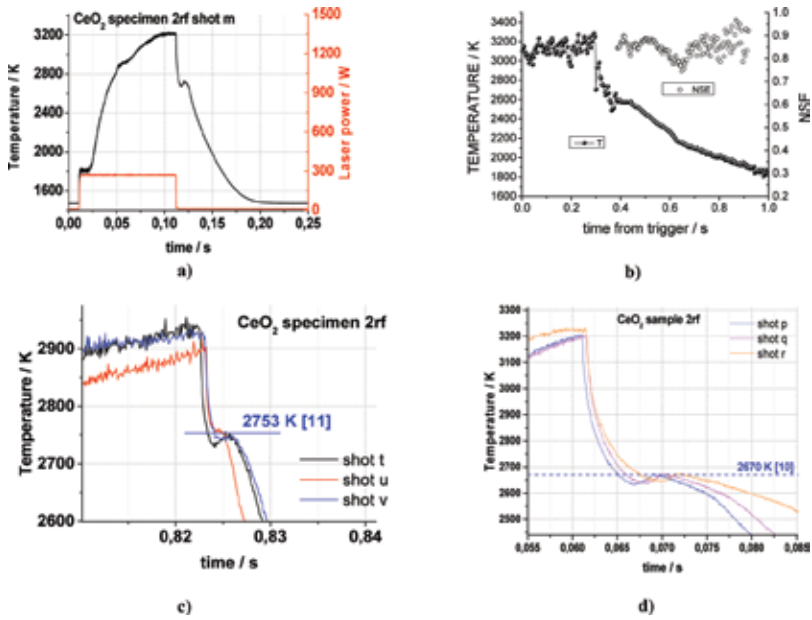

FIGURE 3
Main experiments carried out on sample 2rf. a) Typical thermogram obtained during a laser heating experiment; b) Measurement of normal spectral emissivity (NSE). Each full black circle corresponds to the measurement of a radiance spectrum. Fitting radiance spectra yields the NSE values represented by empty circles in the second part of the experiment. Spectra in the first part of the experiment were very noisy (due to significant vaporisation at high temperature), and could not be fitted successfully. c) Experimental thermal arrests obtained under air at 0.3 MPa; d) Experimental thermal arrests obtained under Ar at 0.3 MPa.

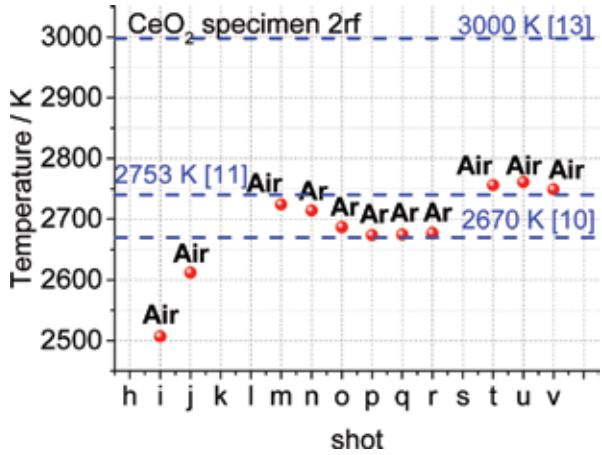

FIGURE 4
Summary of the results obtained in this work on specimen 2rf. Each experimental point is labelled with the atmosphere used during the shot. For comparison, the references melting temperature are reported in the figure, in oxidizing condition (2753 K [11]), reducing (2670 K [10]) and the higher value reported in literature (3000 K [13]).

The experiment reported in fig. 3c was performed using compressed air at 0.3 MPa as buffer gas. The freezing/melting temperature in this experiment is comparable with Foex's results [11].

When argon instead of air was used as buffer gas, lower freezing temperatures were systematically observed. The solidification arrests visible in fig. 3d, for example, occur at a temperature reasonably comparable to the result reported in Mordovin's work [10].

A rather consistent trend for the current CeO_2 data can be observed in fig. 4.

When a sequence of shots under reducing conditions was performed, the temperature tended gradually to reach the value found in Mordovin's work under reducing conditions [10], as indicated by the dashed line. When oxidising instead of reducing conditions were used, the transition temperature tended to the value reported in Foex's work [11].

In the sequence of shots shown in fig. 4, the same trends were reproduced even when alternating the reducing/oxidising atmospheres in successive sets of three to five shots. In some cases two to three shots were needed to stabilise the observed solidification temperature. This confirms even further the systematic effect of the vessel atmosphere, with which the specimen reacts over successive shots until stationary conditions are fully reached resulting in repeatable solidification temperatures from one experiment to the next.

The melting temperatures suggested in this work are (2675 ± 47) K and (2743 ± 33) K for the experiments carried out at 0.3 MPa in Ar and air, respectively.

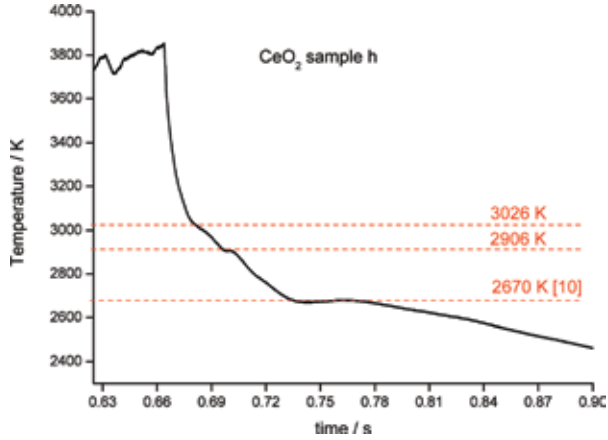

FIGURE 5
Thermogram showing the solidification arrests obtained under a 15 MPa-He-overpressure.

4.2 Laser melting under higher buffer gas pressures

Measurements of the sample surface temperature were more difficult and uncertain under higher buffer gas pressure due to the more complex set-up and the presence of the thick vessel window. For this reason, the melting/freezing temperatures measured under high pressure do not show a specific and well defined trend as the "low" pressure results.

Nonetheless, as expected due to slower vaporisation, phase transition-induced thermal arrests were observed here at higher temperature under high buffer gas pressure, compared with results obtained at pressures close to atmospheric.

In fig. 5 a solidification curve is shown, recorded on a CeO_2 sample laser melted under a He pressure of 15 MPa. Due to the rather poor repeatability of such complex cooling curves, uncertainty bands could not be rigorously defined for the transition temperatures observed in them. However various inflections are visible here, which are interesting in indicating the material behaviour under these conditions far from the ambient ones. The first inflection occurs around 3026 K, and can reasonably be attributed to freezing. It is in fact very unlikely to observe a boiling/condensation transition under this high pressure. The boiling/condensation transition occurs in cerium dioxide at different temperatures depending on the composition of the condensed phase and it is therefore extremely difficult to estimate and observe. The Pu-O phase diagram reported in figure 1b [7], shows that plutonia is expected to boil around 3300 K at the congruent melting composition, which is certainly hypostoichiometric with respect to $PuO_{2.00}$. By analogy of behaviour, a similar boiling temperature can be assumed, in a very first approximation, for ceria. One should however bear in mind that solid/liquid/gas equilibria can be

very complex and largely depend on the experimental conditions in these compounds for which high-temperature phase transitions are strongly non-congruent. This type of complex behaviour in fluorite-like oxides has been recently assessed only for uranium dioxide [21].
A second inflection appears at 2906 K and finally a long plateau at 2679 K. Although the attribution of the last two inflections is difficult, they can certainly be related to the complex Ce-O phase diagram, where the formation of several similar oxygen-deficient phases have been assessed up to high temperatures [9]. It should be noted that such inflections cannot be directly related to the phase boundaries reported in figure 1a, because these have been optimised with an equilibrium total vapour pressure of 1 bar (0.1 MPa). The current results have been obtained under a much higher buffer gas pressure, where phase transitions can occur at considerably different compositions and temperatures. The present data points, in this respect, are more indicative of these trends of the phase boundaries, and should be compared with those obtained, for example, by Tromble [12] and Brewer [13].

5 DISCUSSION

The current results confirm in a clear way that the melting behaviour of cerium dioxide is strongly influenced by the environment and the experimental conditions in which melting occurs. Results obtained under oxidising and reducing atmospheres at pressures slightly exceeding atmospheric confirm those already obtained by Foex with a solar furnace technique [11]. It was already observed in the current investigation, that the resulting melted and refrozen area on the specimen was black, as in all the shots where the melting temperature was exceeded (figure 6b). Figure 6a shows pieces of unmolten sample, of a bright white colour. This behaviour, already observed in other high-melting oxides such as CaO [22] can be ascribed to the formation of oxygen defects, probably related to oxygen losses also leading to some changes in the crystalline structure of the specimen.
The fact that some thermal arrests occur around 2570 K (first tests in figure 4, before stabilisation of the melting/freezing temperatures), close to the monotectic temperature reported in figure 1a for melting CeO_{2-x} in an equilibrium total vapour pressure of 1 bar (0.1 MPa) might be not accidental. However, it should be pointed out once more that the present experimental results should not be directly compared with the phase diagram of figure 1a. Like the earlier results by Mordovin [10] and Foex [11], they rather give an idea of how the phase boundaries might evolve when the experimental boundary conditions are changed, with respect to those of figure 1a, in the sense of stabilising a melting oxide composition closer and closer to the O/Ce = 2.00 stoichiometry.

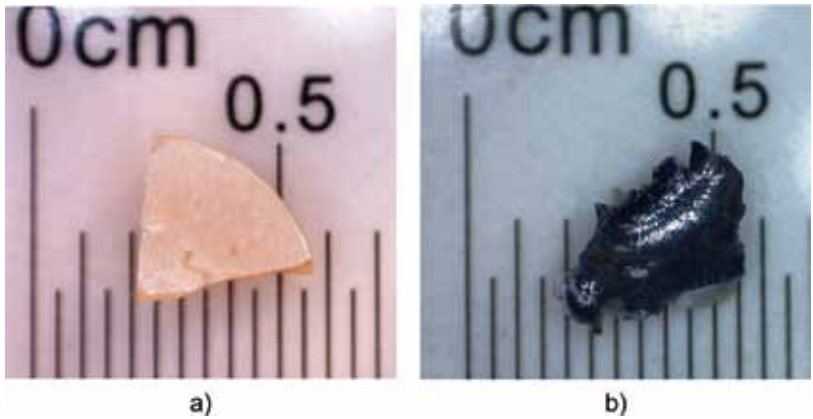

FIGURE 6
CeO_2 sample (fragment) images. a) fresh CeO_2; b) molten CeO_2

The main goal of the current high pressure melting experiments was to limit the formation of oxygen defects, and particularly of the related oxygen losses. For safety reasons, laser heating experiments could not be carried out under an oxygen-containing buffer gas at very high pressure. Such an atmosphere would compensate for oxygen losses, as reported by Tromble [12], although in [12] there is only a scanty description of experimental details. In the present investigation it was considered that a similar effect could be obtained with high enough pressure of inert gas, acting in the sense of slowing the vaporisation kinetics and therefore limiting the oxygen losses and the formation of defects during the experiment. The example thermogram recorded under helium pressurised at 15 MPa (figure 5) shows that a solidification arrest is actually observed at a much higher temperature in this case, exceeding 3000 K. This thermal arrest temperature can be compared with the value given by the Clausius Clapeyron equation for the coexistence of liquid and solid in CeO_2:

$$\frac{dT_m}{dP} = \frac{\Delta H_m}{T_m \cdot \Delta v_m} \tag{2}$$

In (2), T_m is the melting/freezing temperature, P the pressure, ΔH_m the melting enthalpy and Δv_m the specific volume change upon melting. By substituting literature values [9] for these parameters one can easily estimate that the melting point increase due to an overpressure of 15 MPa in CeO_2 should be limited to a few degrees, assuming, as is implicit in Clausius-Clapeyron's equation, that the compound melts congruently. However, the melting point increase recorded here amounts to a few hundreds K. Such an observation constitutes evidence that near-stoichiometric CeO_2 does not melt congruently

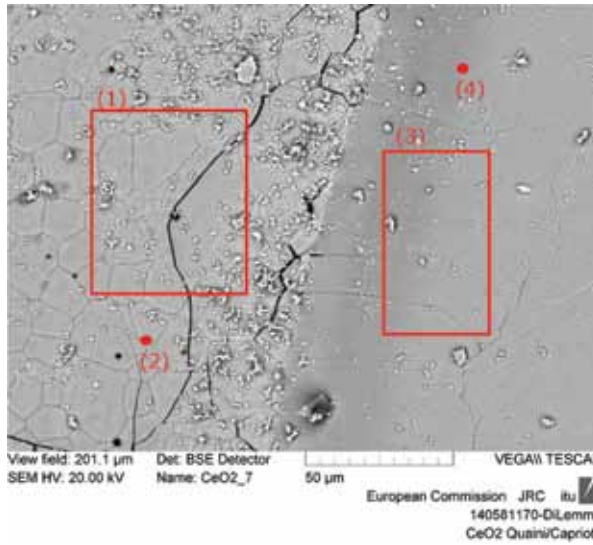

FIGURE 7
SEM back scattering electrons image showing the border between molten (right hand side) and unmolten (left hand side) CeO_2 sample. In red the areas and points measured by EDX analysis and reported in Table 1

TABLE1 1
EDX analysis for melted and unmolten CeO_2. The positions of the EDX spectra (1)–(4) are reported in figure 7.

CeO_2 EDX	**O (at.%)**	**Ce (at.%)**
Melted area (1)	38	62
Melted point (2)	34	66
Unmolten area (3)	63	37
Unmolten point (4)	61	39

(it loses oxygen), even in the current high-pressure experiments. Some oxygen losses and the formation of oxygen defects occur even under these last experimental conditions, as corroborated also by the once more dark colour of the melted/refrozen zone. This is confirmed also by a scanning electron microscope – energy electron spectroscopy (SEM EDX) analysis performed on a ceria sample melted under high pressure of He (Fig. 7). In fig. 7 one can see the boundary between a melted/refrozen zone and the unmelted bulk. Back-scattered electron image and EDX analysis show, qualitatively but consistently, that the melted region is depleted in oxygen with respect to the unmelted one (Table 1).

The presence of three successive thermal arrests in the high pressure experiments can then be interpreted in the light of the Ce-O phase diagram discussion reported by Zinkevitch [9]. Zinkevitch showed that the equilibrium phase diagram is strongly dependent on pressure. Therefore, it is possible that under the current conditions, as opposed to atmospheric pressure heating, part of the investigated material stays closer to the O/Ce = 2.00 stoichiometry throughout the melting/freezing process. This gives the solidification arrest observed in fig. 5 at 3023 K. It should be noted here that there is no way, with the current experimental approach, to prove whether this compound solidifying at the highest observed temperature was actually stoichiometric (O/Ce = 2.00) or not. It is likely, although not certain, that even higher solid/liquid transition temperatures could be obtained under higher pressures or in highly pressurised oxygen (like in the work of Tromble [12]). It is also worth noticing that this solidification arrest at more than 3000 K is poorly repeatable, consistently with the poor chemical stability of CeO_2 at very high temperature. Such material coexists in fact with more reduced phases (lower oxygen content), freezing at lower temperature and giving, upon solidification, the further arrests visible in fig. 5. The final plateau would correspond to the solidification arrest of the most reduced CeO_{2-x} phase, already observed in the low overpressure melting experiments (fig. 3).

Unfortunately, a sound identification of these reduced ceria phases by XRD or other materials characterisation techniques has not been possible in the present work, because of the tiny amount of them produced during the melting/freezing experiments. These phases are mostly cubic and similar in their structure [9]. This makes their identification in the little melted and refrozen material a particularly difficult task, which might be the subject of a further study.

In summary, the present investigation confirms in a single study that the solid/liquid transition occurs in CeO_2 in a non-congruent fashion, accompanied by oxygen losses or, at least, a considerable formation of oxygen defects. These phenomena are strongly dependent on the chemical environment (reducing, oxidising) and the external pressure, and characterise the equilibrium between solid and liquid. As a result, the melting/freezing temperatures are also strongly dependent on pressure and chemical environment. CeO_2 displays therefore in a particularly remarkable way, due to its high oxygen potential [9], a melting behaviour which has been recently proven to be typical of other similar metal-oxygen systems such as Ca-O [22], Np-O [15] and Pu-O [16]. The current results confirm therefore that many similarities exist between the system Pu-O and the system Ce-O, even in the very high temperature behaviour. In particular, based on the present investigation one can expect that neptunium dioxide and plutonium dioxide display slower vaporisation/reduction if heated under a high buffer gas pressure than observed at atmospheric pressure. Further research is needed to confirm this assumption.

6 CONCLUSIONS

The melting behaviour of CeO_2 was investigated here by laser heating under different controlled atmospheres and buffer gas pressures. The effect of the experimental conditions on the detected melting temperature was highlighted. When reducing conditions were used, at pressures close to atmospheric, a melting temperature of $(2675 \pm 47)\,\mathrm{K}$ was obtained. When oxidising conditions were adopted instead, a melting temperature of $(2743 \pm 33)\,\mathrm{K}$ was obtained. The change in the colour of the molten zone may be the post-melting trace of the strong tendency towards reduction of CeO_2. This effect was confirmed even in laser melting experiments performed at high buffer gas pressure up to 15 MPa. In this latter case, however, solidification arrests were obtained at much higher temperatures (around 3026 K), showing that conditions closer to congruent melting could be attained.

ACKNOWLEDGEMENTS

The Authors are indebted to J. Somers, P. Lajarge, F. Di Lemma and P. Raison (JRC ITU) for their help in the sample preparation and characterisation.

REFERENCES

[1] Trovarelli A., Catal. Rev., 38:4 (1996) 439.
[2] Vile´ G., Bridier B., Wichert J., Perez-Ramirez J., Angew. Chem. Int., 51 (2012) 8620.
[3] Yokokawa H., Sakai N., Horita T., Yamaji K., Xiong Y.-P., Fuel Chem. Division Preprints, 47 (2002) 501.
[4] T.L. Markin, R.S. Street, E.C. Crouch, J. Inorg. Nucl. Chem. 32 (1970) 59.
[5] Kim H. S., Joung C. Y., Lee B. H., Oh J. Y., Yang Hyun Koo, Heimgartner P., J. Nucl. Mater. 378 (2008) 98.
[6] Stan M., Zhu Y.T., Jiang H., J. Appl. Phys. 97 (2004) 3358.
[7] Guéneau C., Dupin N., Sundman B., Martial C., Dumas J.-C, Gossè S., Chatain S., De Bruycker F., Manara D., Konings R. J. M., J. Nucl. Mater. 419 (2011) 145.
[8] Stan M. and Cristea P., J. Nucl. Mater. 344 (2005) 213.
[9] Zinkevich M., Djurovic D., Aldinger F., Sol. Stat. Ion., 177 (2006) 989.
[10] Mordovin O. A., Timofeeva N. I., Drozdova L. N., Inorg. Mater. (URSS), 3 (1967) 159.
[11] Foex M., Rev. Hautes Temp. Refract., 3 (1966) 309.
[12] Tromble F., Bull. Soc. Fr. Ceram., 3 (1969) 18.
[13] Brewer L., Chem. Rev., 52 (1953) 1.
[14] Manara D., Sheindlin M., Heinz W., Ronchi C., Rev. Sci. Instrum., 79 (2008) 113901.
[15] Böhler R., Welland M. J., De Bruycker F., Boboridis K., Janssen A., Eloirdi R., Konings R.J.M., Manara D., J. Appl. Phys. 111 (2012) 113501.
[16] De Bruycker F., Boboridis K., Manara D., Poeml P., Rini M., Konings R.J.M., Materials Today 13-11 (2010) 52.
[17] Manara D., Böhler R., Boboridis K., Capriotti L., Quaini A., Luzzi L., Guéneau C., Dupin N., Konings R.J.M., Procedia Chemistry 7 (2012) 505.
[18] Neuer G., Fiessler L., Groll M., Schreiber E., Temperature: Its Measurement and Control in Science and Industry 1992; 6:787–789. J.F. Schooley Editor, AIP New York.
[19] Manara D., PhD Thesis, Technical Note JRC-ITU-TN-2004/05; 2004.

[20] Manara D., Ronchi C., Sheindlin M., High Temp – High Press, 35/36 (2003/2004) 25.
[21] Ronchi C., Iosilevki I.L., Yakub E., «Equation of state of uranium dioxide», Springer – Verlag Berlin Heidelberg 2004.
[22] Manara D., Böhler R., Capriotti L., Quaini A., Bao Z., Boboridis K., Luzzi L., Janssen A., Pöml P., Eloirdi R., Konings R.J.M., J. Eur. Ceram. Soc., 34 (2014) 6 1623.